PARTIAL DISCHARGE PULSE-HEIGHT ANALYSIS - PROMISES AND LIMITATIONS

R. J. Van Brunt, Senior Member, IEEE

National Institute of Standards and Technology
Gaithersburg, Maryland 20899 USA

Abstract – An alternative approach to measurement of the phase-resolved stochastic properties of partial-discharge pulses is described which can be used to unravel significant phase-to-phase memory propagation effects that give rise to nonstationary behavior in the observed pulse-height or phase-of-occurrence distributions. Examples are shown of data obtained using a point-to-dielectric discharge gap.

INTRODUCTION

The measurement of pulse-height distributions is a widely used method for characterizing the statistical behavior of pulsating partial-discharge (PD) phenomena that occur in high-voltage insulation [1]. There has been increasing interest in the use of phase-resolved PD pulse-height and phase-of-occurrence data in providing signatures of different types of PD behavior that can be used for pattern recognition [2–6]. Recent investigations have shown that PD phenomena generated by alternating voltages are generally influenced by significant phase-to-phase memory propagation [7, 9].

The purposes of the present work are: 1) to show how memory propagation complicates the interpretation of phase-resolved pulse-height or phase-of-occurrence distributions and causes such distributions to become susceptible to nonstationary behavior; 2) to show how memory effects can be unraveled by measuring or computing various conditional pulse-amplitude and phase distributions; and 3) to introduce a method for real-time measurement of conditional distributions.

SIGNIFICANCE OF MEMORY PROPAGATION

It can be argued that, in general, pulsating PD phenomena are complex non-Markovian stochastic processes in which memory effects play an important role [8, 9]. Memory effects arise because of the influence of residuals from previous discharge pulses, e.g., surface charge, ion space charge, and species in metastable excited states, on the initiation and development of subsequent discharge pulses. The existence of memory implies that the amplitude and phase of any discharge pulse can depend on the amplitudes and phases-of-occurrence of pulses that occurred at earlier times. Two consequences of memory propagation are: 1) the interpretation of measured PD-pulse amplitude and phase distributions becomes nontrivial, and 2) the phenomena tends to exhibit nonstationary behavior. Nonstationary behavior results in an inability to obtain reproducible data for measured statistical distributions even from "controlled" experiments in which PD's are generated in simple, well defined discharge gaps under ostensibly identical conditions. Because of non-stationary behavior, PD amplitude and phase distributions can exhibit random, unpredictable changes with time. Such unpredictable changes can arise, for example, because of the correlation between PD pulse amplitude and the time that has elapsed since the last PD event. If pulse amplitude and time separation are not independent random variables, then any effect that changes the time distribution between pulses will also change the amplitude distribution.

This is illustrated by previously published data [9] on negative-corona pulses in air shown in Figure 1. The data presented in this figure are measured unconditional corona pulse-amplitude and corresponding time-separation distributions for negative (Trichel-type) corona pulses generated in a simple point-plane gap in which the point electrode is irradiated with ultra-violet light of variable intensity, I_i. In this case, the discharge pulses are initiated primarily by photo-electrons emitted from the point electrode, and therefore, the mean time between pulses will tend to decrease as I_i increases. The normalized time-separation distributions, $p_o(\Delta t_n)$, for different I_i shown in Figure 1 are consistent with this expectation. The corresponding unconditional pulse-amplitude distributions, $p_o(q_n)$, also exhibit significant changes with I_i thus suggesting a dependence of the amplitude, q_n, of the nth pulse on its time separation, Δt_{n-1}, from the previous pulse.

A dependence of q_n on Δt_{n-1} was verified by measuring conditional pulse-amplitude distributions $p_1(q_n|\Delta t_{n-1})$ which give the probability that the nth pulse will have an amplitude q_n if its time separation from the previous pulse has a fixed value Δt_{n-1}. Examples of measured $p_1(q_n|\Delta t_{n-1})$ distributions are shown in Figure 2 in comparison with the corresponding unconditional distribution. The conditional distributions are much narrower than the unconditional distribution and exhibit a dependence on Δt_{n-1}. The dashed line in this figure is the unconditional distribution, $p_o(q_n)$, predicted from the measured distributions, $p_o(\Delta t_{n-1})$ and $p_1(q_n|\Delta t_{n-1})$, using the integral expression

$$p_o(q_n) = \int_o^\infty p_o(\Delta t_{n-1}) p_1(q_n|\Delta t_{n-1}) d(\Delta t_{n-1}). \qquad (1)$$

This expression, which follows from the law of probabilities, indicates how the distributions $p_o(q_n)$ and $p_o(\Delta t_{n-1})$ shown in Figure 1 are related. Measurement of the conditional pulse-amplitude distributions serves to uncouple the dependence of q_n on Δt_{n-1}.

In the case of self-sustained negative corona, the time-interval distribution is determined by the rate of electron release from the cathode surface by field emission and/or secondary processes such as ion impact or quenching of metastable species. The electron release rate is thus strongly dependent on electrode surface conditions which are difficult to control and may, in fact, be changed

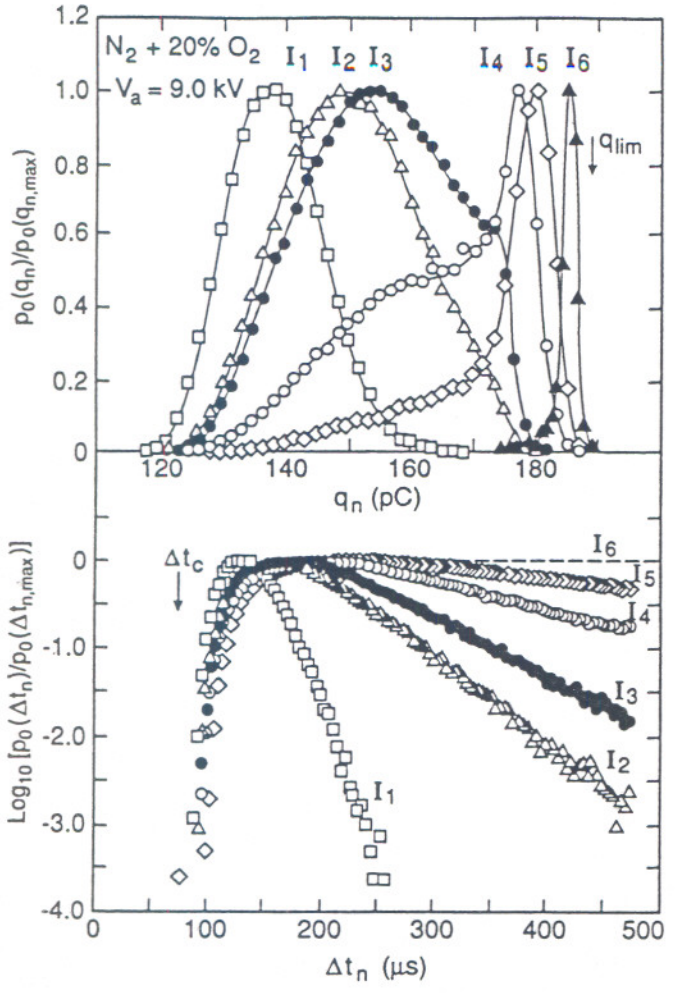

Fig. 1. Measured unconditional Trichel-pulse-amplitude, $p_o(q_n)$, and corresponding pulse-time-separation, $p_o(\Delta t_n)$, distributions at the different indicated relative intensities of *UV* irradiation $I_i(I_1 > I_2 > I_3...)$ for a point-plane gap voltage of 9.0 kV in a 100 - kPa N_2 + 20% O_2 gas mixture.

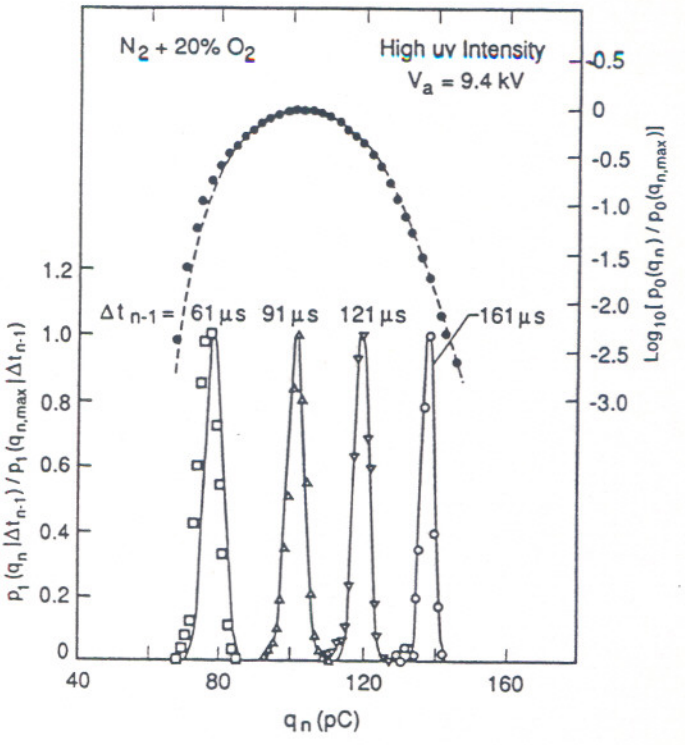

Fig. 2. Measured unconditional $p_o(q_n)$ and corresponding conditional $p_1(q_n|\Delta t_{n-1})$ distributions at 9.4 kV for the indicated values of Δt_{n-1} which apply to Trichel pulses generated in a 100 kPa N_2 + 20% O_2 gas mixture using an irradiated point-plane electrode configuration. The solid lines are Gaussian representations of the p_1 data that were used together with numerical data on the corresponding $p_o(\Delta t_n)$ distribution in Eq. (1) to give the predicted $p_o(q_n)$ indicated by the dashed line [9].

by the discharge process. It is therefore expected that negative-corona pulses will exhibit nonstationary behavior as evident from a lack of reproducibility in previous pulse-height distribution measurements [10].

REAL-TIME STOCHASTIC ANALYZER

Figure 3 shows a block diagram of a stochastic analyzer that is used to measure, in real time, a set of conditional and unconditional pulse-amplitude and phase-of-occurrence distributions. It is an extended version of a previously described device [9, 11] that was used to obtain data such as shown in Figures 1 and 2 on the stochastic properties of dc corona pulses. In addition to the distributions previously measured, the present version allows measurement of many different phase-restricted distributions needed to characterize the stochastic behavior of ac-generated PD's.

Table 1 shows a partial list of the additional phase-restricted distributions that can be measured with this system. The different components that comprise the measurement system are defined in the figure caption. A detailed explanation of how this system works cannot be covered in this brief report. A complete documentation of the system operation together with descriptions of the individual circuits is now in preparation.

Table 1

Conditional (p_1 and p_2) and unconditional (p_o) PD pulse amplitude and phase distributions considered in the present work.

Pulse-Amplitude distributions	Phase-of-occurrence distributions	Phase restrictions
$p_o(q_i^{\pm})$	$p_o(\phi_i^{\pm})$	$\phi_i^{+} \in (-\delta\phi, \pi - \delta\phi)$
		$\phi_i^{-} \in (\pi - \delta\phi, 2\pi - \delta\phi)$
$p_1(q_j^{\pm}\|\Delta\phi_{uJ}^{\pm})$	$p_1(\phi_j^{\pm}\|\Delta\phi_{uJ}^{\pm})$	$\Delta\phi_{uJ}^{\pm} = \phi_u^{\pm} - \phi_l^{\mp}$
		$\phi_j^{\pm} \in (\phi_l^{\mp}, \phi_u^{\pm})$
$p_1(q_i^{\mp}\|Q^{\pm})$	$p_1(\phi_i^{\mp}\|Q^{\pm})$	$Q^{\pm} = \sum_k q_k^{\mp}(\phi_k^{\mp})$
$p_2(q_i^{\pm}\|Q^{\mp}, \phi_i^{\mp})$		$\phi_k^{+} \in (-\delta\phi, \pi - \delta\phi)$
		$\phi_k^{-} \in (-\pi - \delta\phi, -\delta\phi)$
		$i = 1, 2, 3, \cdots$
		$j \geq 1, k \geq 1$

Figures 4 and 5 show pulse diagrams for the different circuit locations in Figure 3 that apply respectively to the measurement of the conditional distributions $p_1(\phi_i^{\pm}|Q^{\mp})$ and $p_2(q_1^{\pm}|o_1^{\pm}, Q^{\mp})$ for which examples of data are shown in the next section. The notation used here is like that previously defined [7, 8]. For example, ϕ_i^- is the phase-of-occurrence of the i th pulse on the negative half-cycle, q_1^+ is the amplitude of the first pulse on the positive half-cycle, and Q^+ is the net charge associated with all pulses that occur in a positive half-cycle, i.e.,

$$Q^+ = \sum_i q_i^+. \tag{2}$$

Shown in Table 2 are the combinations of switch configurations (S1–S4 in Figure 3) that are required to measure the distributions $p_o(\phi_i^{\pm})$, $p_1(\phi_i^{\pm}|Q^{\mp})$, and $p_2(q_1^{\pm}|\phi_1^{\pm}, Q^{\mp})$. It is also possible to configure the system in other ways to measure many other conditional distributions such as, for example, $p_2(\phi_i^-|q_{i-1}^-, \phi_{i-1}^-)$, $p_2(q_i^-|\phi_{i-1}^-, \phi_i^- - \phi_{i-1}^-)$, and $p_1(\phi_{ij}^-|Q_{j-k}^+), j \geq k$. In the latter distribution, ϕ_{ij}^- is the phase-of-occurrence of the i th pulse in the j th negative half-cycle and Q_{j-k}^+ is the net charge from all PD's on the $(j-k)$ th positive half-cycle. The conditional distributions indicated in Table 2 were selected for consideration here because they can be interpretted easily and unambiguously in terms of expected memory propagation from half-cycle to half-cycle.

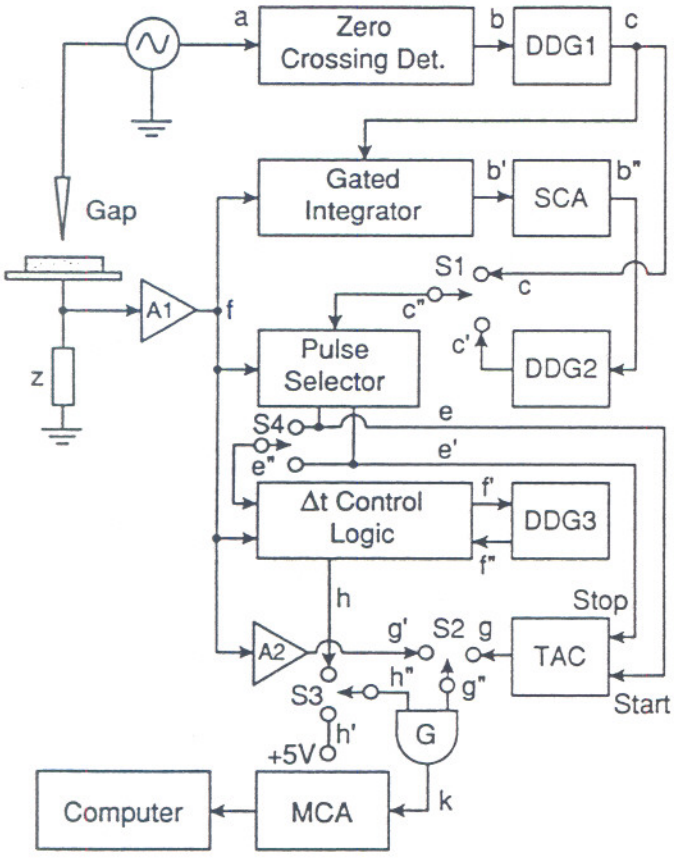

Fig. 3. Stochastic analyzer. The individual components are defined as follows: A-amplifier, G-gate, S-switch, DDG-digital delay pulse generator, MCA-multichannel analyzer, SCA-single channel analyzer, TAC- time-to-amplitude converter. The Δt control logic circuit is similar to that previously described [11].

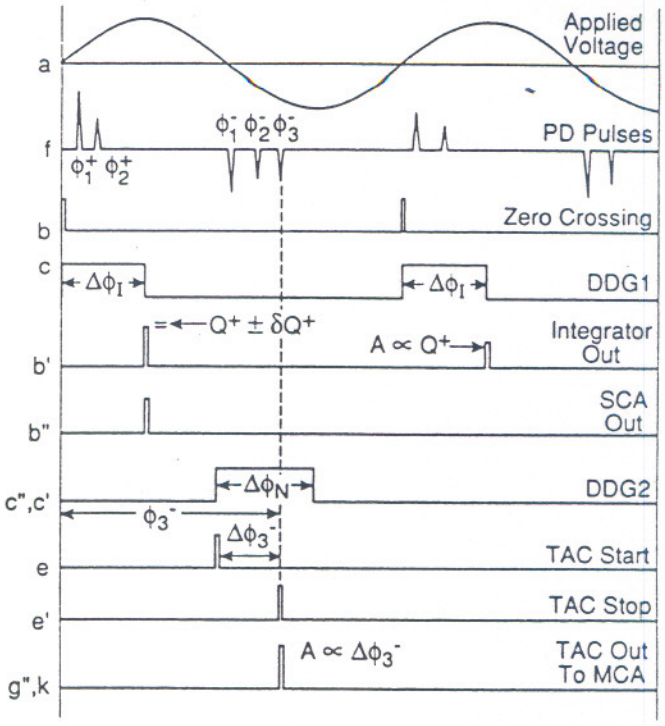

Fig. 4. Pulse diagram corresponding to the different indicated circuit points in Figure 3 for measurement of $p_1(\phi_3^-|Q^+)$.

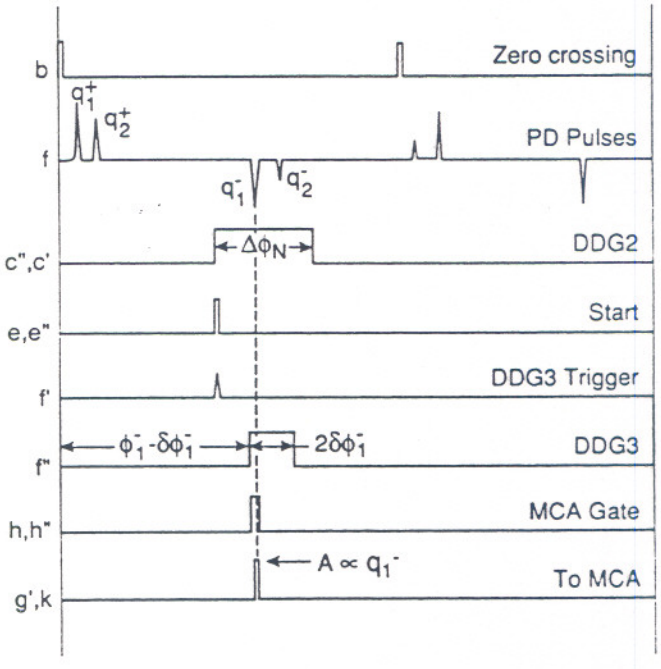

Fig. 5. Pulse diagram for measurement of $p_2(q_1^-|Q^+, o_1^-)$.

EXAMPLES

Shown in Figures 6 and 7 are examples of measured conditional distributions $p_1(\phi_i^-|Q^+), i = 1, 8, 16$ and $p_2(q_1^+|o_1^+, Q^-)$ that clearly demonstrate the existence of significant memory propagation between successive half-cycles of the applied ac voltage. The measurements were performed using a 200 Hz, 3.0 kV rms volt-

Table 2 - Configuration of switches in Figure 3 for measurement of the different indicated distributions

Switch	$p_o(\phi_i^{\pm})$ $i = 1, 2, \ldots$	$p_1(\phi_i^{\pm}\|Q^{\mp})$ $i = 1, 2, \ldots$	$p_2(q_1^{\pm}\|Q^{\mp}, \phi_i^{\pm})$
S1	$c'' = c$	$c'' = c'$	$c'' = c'$
S2	$g'' = g$	$g'' = g$	$g'' = g'$
S3	$h'' = h'$	$h'' = h'$	$h'' = h$
S4	—	—	$c'' = e$

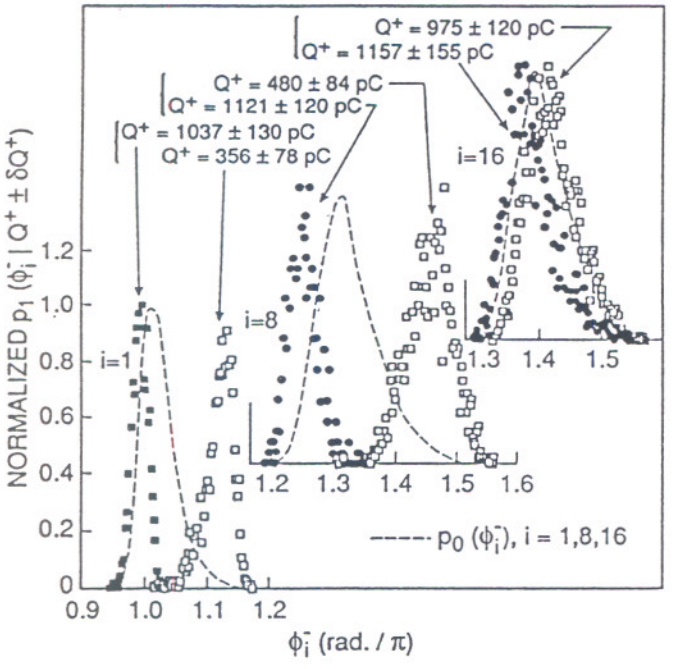

Fig. 6. Measured conditional and unconditional phase-of-occurrence distributions for the 1st, 8th, and 16th pulses in the negative half-cycle.

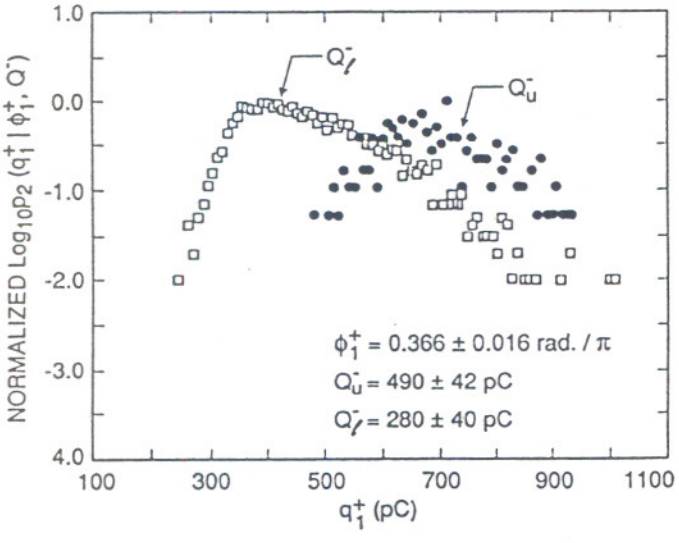

Fig. 7. Measured second-order conditional pulse-amplitude distribution of the first pulse in the positive half-cycle.

age applied to a point-to-dielectric gap similar in configuration to that used previously [7, 12]. The dielectric was a flat, rectangular, 1 mm thick, section of polytetrafluorocthylene (PTFE) attached to a planar metal surface. The stainless-steel point electrode had a radius of curvature at the tip of about 0.05 mm and could be moved relative to the PTFE to give different gap spacings in room air. For the data shown in Figure 6, the gap spacing was 1.5 mm, and for the data in Figure 7, the spacing was zero, i.e., the point touched the PTFE surface.

The data in Figure 6 correspond to Trichel-like negative-corona pulses that are known to occur in point-dielectric gaps even at very small gap spacings [12]. Twenty or more Trichel pulses could occur in a single half-cycle under the conditions that apply to this figure. Shown in Figure 6 are both conditional and unconditional phase-of-occurrence distributions for the 1st, 8th, and 16th pulses in the negative half-cycle. For the conditional distributions, the net charge associated with PD's in the previous positive half-cycle are restricted to lie within the indicated ranges. The relationship between the unconditional and conditional distributions shown here is discussed in the next section.

The data shown in Figure 7 correspond to a second order conditional amplitude distribution of the first pulse on the positive half-cycle conditioned on the indicated range of values for Q^- and ϕ_1^+. In this case the PD phenomenon is a dielectric surface discharge like that previously considered [7, 8].

DISCUSSION AND CONCLUSIONS

The data in Figure 6 indicate that the larger the amount of charge deposited on the dielectric surface by PD events in a positive half-cycle the sooner will be the occurrence of PD pulses in the subsequent negative half-cycle. This trend is consistent with predictions of a simple model for PD formation in dielectric barrier gaps previously discussed [7, 8]. It is interesting to note that memory of the charge deposited during the previous half-cycle is retained even at the 16th pulse.

The distributions shown in Figure 7 are also consistent with the model and with previously reported data for pulses in the negative half-cycle [8]. They indicate that as Q^- increases, the mean amplitude of the first pulse to occur on the positive half-cycle at a particular phase will also increase. The results shown in both figures clearly demonstrate the importance of memory effects in influencing the stochastic behavior of PD pulses. The effects can be expected to occur in any gap configuration where dielectric surfaces are present.

The implications of memory effects revealed here on the interpretation of conditional phase-resolved measurements reported by others [2-6] will now be considered. The unconditional phase-of-occurrence distributions as shown by the dashed lines in Figure 6 are related to the conditional distributions by an integral expression similar to Eq. 1, namely

$$p_o(\phi_i^{\pm}) = \int_o^{\infty} p_o(Q^{\mp}) p_1(\phi_i^{\pm}|Q^{\mp}) dQ^{\mp}, \qquad (3)$$

where $p_o(Q^{\mp})dQ^{\mp}$ is the probability that the net PD charge in the previous half-cycle will lie in the range $Q^{\mp}$ to $Q^{\mp}+dQ^{\mp}$. For $i > 1$, the occurrence of the i th pulse may depend on previous pulses that occurred in the same half-cycle. Taking this into account in the case, for example, of the second pulse gives

$$p_o(\phi_2^{\pm}) = \int_o^{\infty} \int_{\phi'-\delta\phi}^{\phi'+\pi} \int_o^{\infty} p_o(Q^{\mp}) p_1(\phi_1^{\pm}|Q^{\mp}) p_2(q_1^{\pm}|Q^{\mp}, \phi_1^{\pm}) \times p_3(\phi_2^{\pm}|Q^{\mp}, \phi_1^{\pm}, q_1^{\pm}) dQ^{\mp} d\phi_1^{\pm} dq_1^{\pm}, \quad (4)$$

where $\phi' = 0$ or π for positive or negative half-cycles respectively, and a small phase-shift, $\delta\phi$, is introduced to allow for the possibility that a pulse may actually occur slightly before the voltage zero-crossing as is the case for the $i = 1$ data in Figure 6. Similar, but more complex, integral expression involving higher order conditional distributions can be written for $p_o(\phi_i^{\pm}), i > 2$.

The unconditional phase-resolved distribution of PD events in a particular half-cycle is given by

$$p_o(\phi^{\pm} \in \Delta\phi^{\pm}) = \frac{1}{M} \sum_{j=1}^{M} \sum_{i=1}^{N} p'_{ij} \int_{\Delta\phi^{\pm}} p_o(\phi_i^{\pm}) d\phi_i^{\pm}, \quad (5)$$

where $p_o(\phi^{\pm} \in \Delta\phi^{\pm})\Delta\phi^{\pm}$ is the probability that any event will occur in the phase interval $\Delta\phi^{\pm}$, p'_{ij} is the probability that an i th pulse will actually occur in the j th half-cycle, and averages have been performed over M cycles and over the phase window selected. The p'_{ij} can be viewed as weighting factors for the distributions $p_o(\phi_i^{\pm})$ such as given by Eq. 4.

The phase-resolved amplitude distribution for the first pulse in a given half-cycle is related to distributions shown in Figures 6 and 7 by

$$p_1(q_1^{\pm}|\phi_1^{\pm} \in \Delta\phi^{\pm}) = \int_{\Delta\phi^{\pm}} \int_o^{\infty} p_o(Q^{\mp}) p_1(\phi_1^{\pm}|Q^{\mp}) \times p_2(q_1^{\pm}|Q^{\mp}, \phi_1^{\pm}) dQ^{\mp} d\phi_1^{\pm}. \quad (6)$$

More complex integral expressions are found for $i > 1$. The unconditional phase-resolved pulse-height distribution is then given by

$$p(q_i^{\pm}; \phi_i \in \Delta\phi^{\pm})_{i\geq 1} = \frac{1}{M} \sum_{j=1}^{M} \sum_{i=1}^{N} p'_{ij} \int_{\Delta\phi^{\pm}} p_o(\phi_i^{\pm}) p_1(q_i^{\pm}|\phi_i^{\pm}) d\phi_i^{\pm}. \quad (7)$$

Equations (5) and (7) indicate the formidable difficulties to be encountered in the interpretation of unconditional phase-resolved PD data. It can thus be argued from the information presented here that measurement of conditional distributions not only provides more insight into the physics of PD phenomena but may also be more useful for pattern recognition purposes. In general, conditional distributions are more immune to nonstationary behavior than unconditional distributions.

ACKNOWLEDGEMENTS

Valuable contributions to this work were made by E. W. Cernyar, a coop student from Georgia Tech, S. V. Kulkarni now of the Institute for Plasma Research in India, and P. von Glahn of Villanova University. Partial support was provided by the U. S. Department of Energy, Office of Energy Storage and Distribution.

REFERENCES

[1] R. Bartnikas, "A Commentary on Partial Discharge Measurement and Detection," IEEE Trans. Elec. Insul., vol. EI-21, pp. 629-653, 1987.

[2] T. Okamoto and T. Tanaka, "Novel Partial Discharge Measurement-Computer-Aided Measurement Systems," IEEE Trans. Elec. Insul., vol. EI-21, pp. 1015-1016, 1986.

[3] E. Gulski and F. H. Kreuger, "Computer-aided Analysis of Discharge Patterns," J. Phys. D: Appl. Phys., vol. 23, pp. 1569-1575, 1990.

[4] E. Gulski, P. H. F. Morshuis, and F. H. Kreuger, "Atomized Recognition of Partial Discharges in Cavities," Japanese J. Appl. Phys., vol. 29, pp. 1329-1335, 1990.

[5] M. Hikita, Y. Yamada, A. Nakamura, T. Mizutani, A. Oohasi and M. Ieda, "Measurement of Partial Discharges by Computer and Analysis of Partial Discharge Distribution by the Monte Carlo Method," IEEE Trans. Elec. Insul., vol. 25, pp. 453-468, 1990.

[6] J. M. Braun, S. Rizzetto, N. Fujimoto, and G. L. Ford, "Modulation of Partial Discharge Activity in GIS Insulators by X-ray Irradiation," IEEE Trans. Elect. Insul., vol. 26, pp. 460-468, 1991.

[7] R. J. Van Brunt and E. W. Cernyar, "Influence of Memory Propagation on Phase-Resolved Stochastic Behavior of AC-Generated Partial Discharges," Appl. Phys. Lett., vol. 48, pp. 2628-2630, 1991.

[8] R. J. Van Brunt, "Stochastic Properties of Partial-Discharge Phenomena," IEEE Tran. Elec. Insul., vol. 26, Oct. 1991.

[9] R. J. Van Brunt and S. V. Kulkarni, "Stochastic Properties of Trichel-Pulse Corona: A Non-Markovian Random Point Process," Phys. Rev. A, vol. 42, pp. 4908-4932, 1990.

[10] N. H. Malik and A. A. Al-Arainy, "Statistical Variation of DC Corona Pulse Amplitudes in Point-to-Plane Air Gaps," IEEE Trans. Elec. Insul., vol. 22, pp. 825-829, 1987.

[11] R. J. Van Brunt and S. V. Kulkarni, "Method for Measuring the Stochastic Properties of Corona and Partial-Discharge Pulses," Rev. Sci. Instrum., vol. 60, pp. 3012-3023, 1989.

[12] R. J. Van Brunt, M. Misakian, S. V. Kulkarni, and V. K. Lakdawala, "Influence of a Dielectric Barrier on the Stochastic Behavior of Trichel-pulse Corona," IEEE Trans. Elec. Insul., vol. 26, pp. 405-415, 1991.